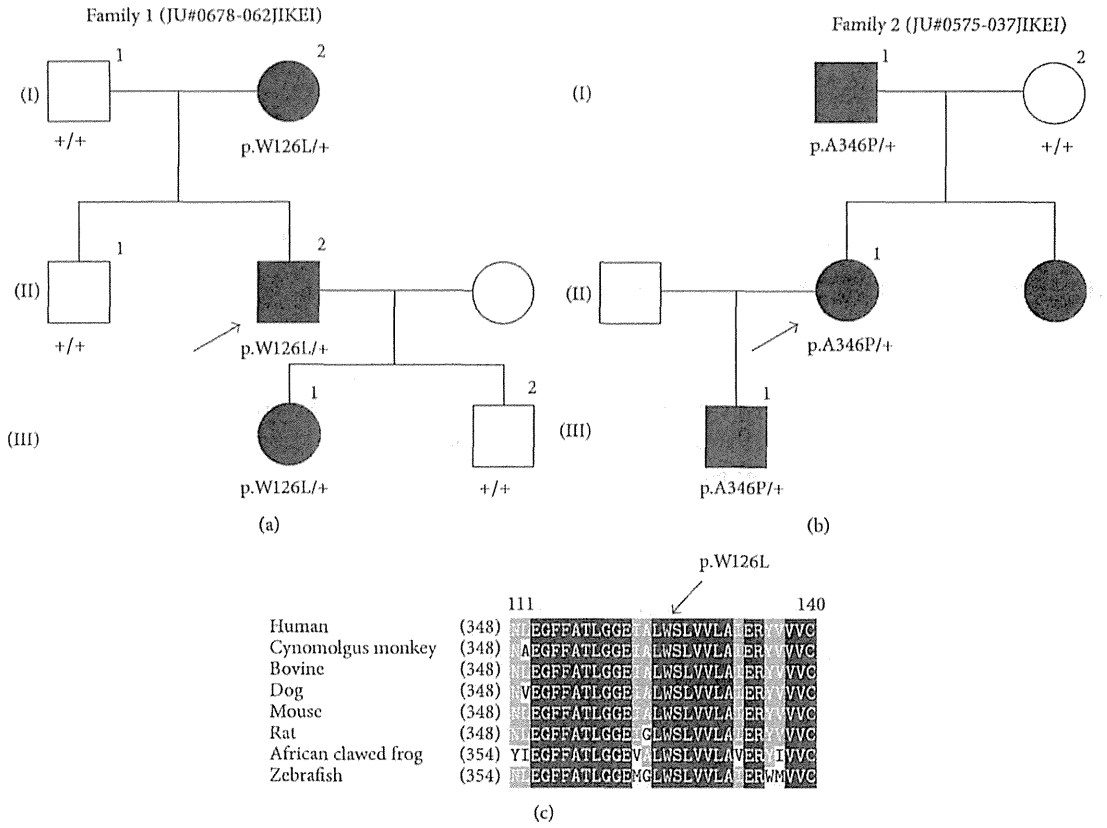

FIGURE 1: Pedigrees of the two Japanese families with RP and amino acid sequence alignment of the rhodopsin in different vertebrate species. (a) and (b) The solid squares (male) and circles (female) represent the affected individuals. The proband of each family is indicated by the arrows. (c) The tryptophan residue at position 126 is highly conserved. The conserved amino acids between the different species are shown in the black boxes. The less and least conserved amino acids are highlighted in the gray or white boxes, respectively.

Dominant (or heterozygous) *RHO* mutations have been reported to show two different RP phenotypes, classic RP and sector RP [8–12]. Classic RP is a typical form of RP that is characterized by early-onset and diffuse/generalized retinal dysfunction, whereas sector RP is characterized by adult-onset and regionalized/sectorial retinal dysfunction [13–15]. Sector RP, as originally described by Bietti in 1937 [16], is characterized by retinal degeneration that is limited to one or two quadrants of the fundus and slowly progression compared with classic RP [13–15].

The frequency of the *RHO* mutations in adRP differs between ethnic groups. For example, there is a much lower frequency of *RHO* mutations in Japanese, Chinese, and Korean populations compared with European populations [17–19]. Saga et al. found *RHO* mutations in 1/13 (7.7%) adRP Japanese patients [20], whereas a separate study found that 43/150 (29%) adRP patients in North America had the *RHO* mutations [21]. Thus, *RHO* mutations have not been considered a major cause of adRP in Japanese patients.

To date, only a small number of *RHO* mutations have been reported in the Japanese population [20, 22–25]. In our current study, we used a whole-exome sequencing technique and identified two *RHO* mutations in two Japanese families with adRP, one (p.W126L) of which was novel. We additionally examined the impact of the p.W126L mutation on rhodopsin conformation by investigating the molecular modeling.

2. Material and Methods

The protocol of this study was approved by the Institutional Research Board of The Jikei University School of Medicine and National Hospital Organization Tokyo Medical Center. The protocol adhered to the tenets of the Declaration of Helsinki, and informed consent was obtained from all participants.

2.1. Clinical Studies. Ten unrelated adRP patients from ten Japanese families were recruited for this study. RP diagnosis was based on the visual field, fundus examination, and electroretinogram (ERG) findings. Detailed ophthalmic examinations were conducted in the two families that exhibited the *RHO* mutations (family 1: JU#0678-062JIKEI and family 2: JU#0575-037JIKEI) (Figures 1(a) and 1(b)). These evaluations included decimal best-corrected visual acuity (BCVA), slit-lamp, and fundus examinations, optical coherence tomography (OCT) (Cirrus HD-OCT; Carl Zeiss Meditec AG,

Dublin, CA), and fundus autofluorescence imaging (Spectralis HRA; Heidelberg Engineering, Heidelberg, Germany). Visual fields were assessed with kinetic Goldmann perimetry (GP; Haag Streit, Bern, Switzerland). Full-field ERG was performed according to the protocols of the International Society for Clinical Electrophysiology of Vision. Details of the methods and normal data have been reported previously [26].

2.2. DNA Preparation and Exome Sequencing Analysis. After obtaining venous blood samples from ten adRP patients, genomic DNA was extracted. Whole-exome sequencing was performed in all ten adRP patients using a previously described method [27]. The obtained sequence data in the patients were compared with reference human genome sequences (1000 genomes phase 2 reference, hs37d5). Subsequently, we then focused on only the variants that could change the amino acid sequence, such as the nonsynonymous variants, splice acceptor, and donor site variants, and the short insertions and deletions. In the next step, we filtered the remaining variants using the criteria that the frequency of the variant had to be less than 1% in the databases of the 1000 Genomes project (http://www.1000genomes.org) and the Human Genetic Variation Browser (http://www.genome.med.kyoto-u.ac.jp/SnpDB/index.html). In the final step, we screened variants residing within the 212 retinal disease-associated genes listed in the RetNet database that was last updated on March 10, 2014 (https://sph.uth.edu/retnet/).

2.3. Sanger Sequencing for RHO Mutations. Sanger sequencing for *RHO* mutations was conducted in two of the Japanese families, which included probands and other family members (Figures 1(a) and 1(b)). We used two primer pairs: a forward primer (RHO-2F), 5′-CTCCTCAAATCCCTCTCCCACTCCT-3′, and a reverse primer (RHO-2R), 5′-TCTTCTGCCCTACACCCCTACCCTG-3′ for exon 2, and a forward primer (RHO-5F), 5′-CGAACCTCACTAACGTGCCAG-3′, and a reverse primer (RHO-5R), 5′-GGTCTTGGTGGATGTCCCTTC-3′ for exon 5.

2.4. Molecular Modeling and Simulation. The models for molecular dynamics (MD) simulation were generated using two bovine rhodopsin/opsin crystal structures as the templates: the dark-adapted rhodopsin (Protein Data Bank ID: 1U19, chain A) and the ligand-free form opsin (Protein Data Bank ID: 3CAP, chain A). To examine the impact of the p.W126L mutation on protein conformation, 11-*cis*-retinal was removed from the dark-adapted template. Amino acids in these templates were replaced with the corresponding amino acids from the human sequence, thereby resulting in the wild-type (WT) models. The p.W126L models were generated from the WT models by changing the tryptophan at position 126 to leucine. All amino acid replacements were performed by using the simple mutate function of the Coot software [28]. The membrane environment was an artificially generated palmitoyl-oleoyl-phosphatidyl choline bilayer of approximately 120 molecules with a dimension of 80 × 80 Å. Each model was then merged with the membrane. All of the models we developed were superposed onto each other so that each model was embedded in the artificial membrane at almost identical orientations. The protein-membrane system was then solvated with water containing 150 mM NaCl. All manipulations were performed using Visual Molecular Dynamics version 1.9 [29].

MD simulations were run by the Not (just) Another Molecular Dynamics program [30] through the visual molecular dynamics interface using the following conditions: 1 fs per step, 100,000 steps (100 ps) for minimization, and 1,000,000 steps (1 ns), periodic boundary conditions and particle mesh Ewald method [31], cut-off at 10 Å, and switching at 9 Å. The calculations were carried out under a constant pressure and temperature ensemble at 310 K and 1 bar. A figure was prepared using the Discovery Studio Visualizer software (Accelrys Inc., San Diego, CA).

3. Results

3.1. Clinical Findings in Family 1 (JU#0678-062JIKEI)

3.1.1. Patient II-2. Patient II-2 (a proband) was a 58-year-old man, who was referred to our hospital because of suspicion of RP. BCVA at his first visit to our hospital was 1.5 (with +1.50 diopter (dpt), cylinder (cyl) −1.25 dpt axial (Ax) 20°) in his right eye and 0.7 (with +1.50 dpt., cyl. −0.50 dpt. Ax. 150°) in his left eye. No abnormalities were found except for slight senile cataracts in the anterior segments and media of both eyes. Intraocular pressures were within the normal range in both eyes. Fundus examination revealed retinal degeneration around the inferior vascular arcade in his right (Figure 2(a)) and left eyes. The OCT images showed marked thinning of the outer nuclear layer (ONL) and disruption of the inner segment/outer segment (IS/OS) line, except for the foveal region of his right (Figure 2(a)) and left eyes. GP at a previous hospital showed depression of visual fields and an arcuate scotoma at the superior visual field in his right (Figure 2(a)) and left eyes. Full-field ERG showed that there were decreased amplitudes in the rod, standard combined, cone, and 30-Hz flicker responses (Figure 3(a)).

3.1.2. Patient III-1 (a Daughter of Patient II-2). Patient III-1 was a 31-year-old woman, who reported night blindness. The clinical findings of patient III-1 were essentially similar to those found for patient II-2. BCVA at her first visit to our hospital was 1.5 (with cyl. −0.50 dpt. Ax. 160°) in her right eye and 1.2 (with cyl. −1.00 dpt. Ax. 35°) in her left eye. There were no abnormalities found in the anterior segments and media of either eye. Intraocular pressures were within the normal range in both eyes. Fundus examination revealed retinal degeneration in the nasal area of her right (Figure 2(b)) and left eyes. The OCT images showed marked thinning of the ONL and disruption of the IS/OS line except for the foveal region of her right (Figure 2(b)) and left eyes. GP showed several isolated scotomas in her right (Figure 2(b)) and left eyes. Full-field ERG showed that there were decreased amplitudes in the rod, standard combined, cone, and 30-Hz flicker responses (Figure 3(b)).

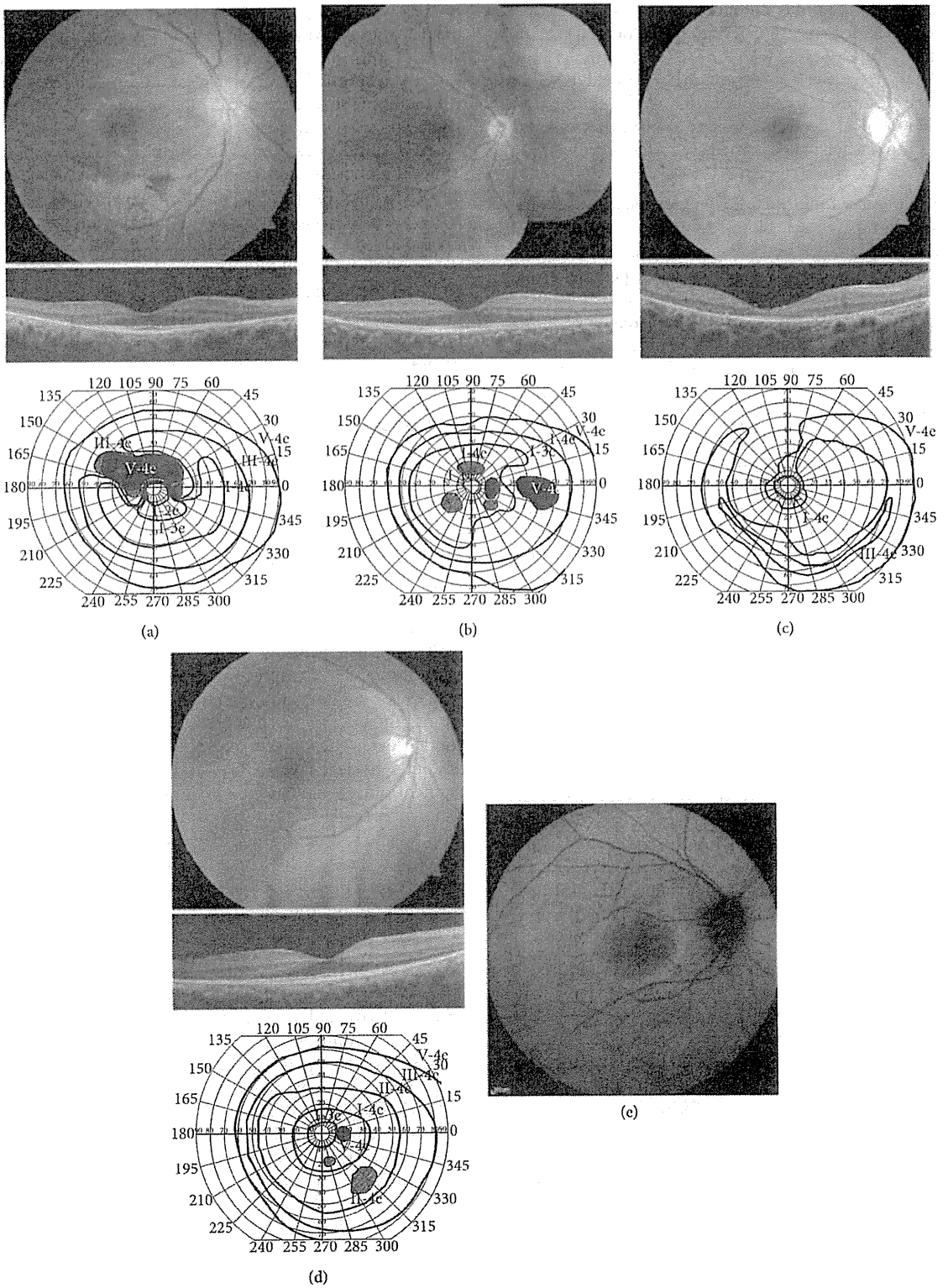

Figure 2: Fundus photographs, optical coherence tomography (OCT) images, and visual fields with Goldmann kinetic perimetry (GP) for the two Japanese families with retinitis pigmentosa. (a) Fundus photograph, OCT, and GP in the right eye of patient II-2 in family 1. (b) Fundus photograph, OCT, and GP in the right eye of patient III-1 in family 1. (c) Fundus photograph, OCT, and GP in the right eye of patient II-1 in family 2. (d) Fundus photograph, OCT, and GP in the right eye of patient III-1 in family 2. (e) A fundus autofluorescence image in the right eye of patient III-1 in family 2. See the Results section for details.

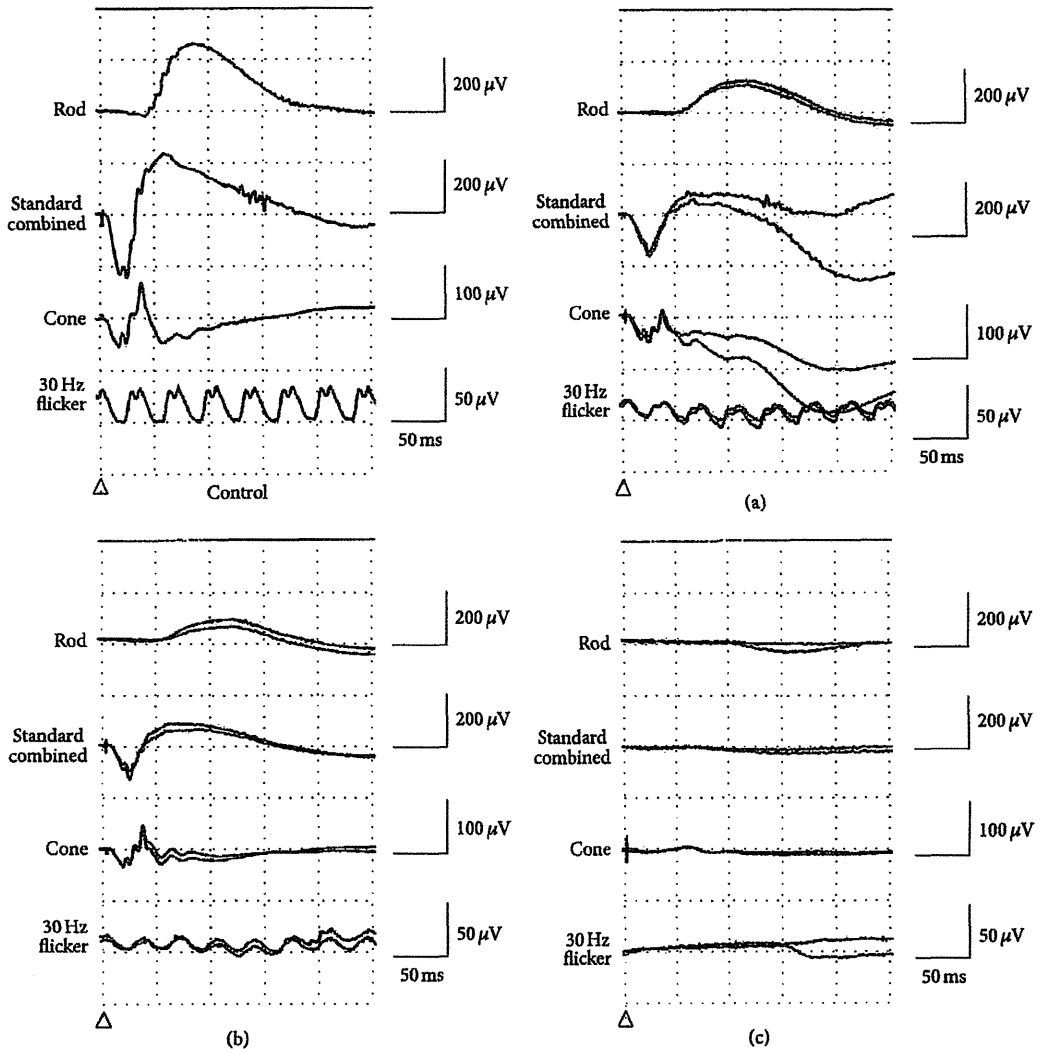

FIGURE 3: Full-field electroretinograms (ERGs). (a) and (b) ERG of both patient II-2 (a) and patient III-1 (b) in family 1 shows diminished amplitudes of the rod, standard combined, cone, and 30-Hz flicker responses. (c) ERG of patient II-1 in family 2 is nonrecordable for the rod, standard combined and 30-Hz flicker responses.

3.2. *Clinical Findings in Family 2 (JU#0575-037JIKEI)*

3.2.1. Patient II-1. Patient II-1 (a proband) was a 35-year-old woman referred to our hospital for assessment of a causative gene for her RP. BCVA was 0.7 (with no correction) in her right eye and 0.6 (with cyl. −1.75 dpt. Ax. 30°) in her left eye. There were no abnormalities found in the anterior segments and media of either eye. Intraocular pressures were within the normal range in both eyes. Fundus examination revealed diffuse retinal degeneration and intraretinal pigment deposits with a bone-spicule configuration around the vascular arcade to the periphery of her right (Figure 2(c)) and left eyes. The OCT images showed marked thinning of the ONL and entire disruption of the IS/OS line in her right (Figure 2(c)) and left eyes. GP showed a ring-like defect in her right (Figure 2(c)) and left eyes. Full-field ERG showed that there were no responses in the rod, standard combined, and 30-Hz flicker ERG (Figure 3(c)).

3.2.2. Patient III-1 (a Son of Patient II-1). Patient III-1 was a 14-year-old boy, who was first found to have night blindness at 6 years of age. At the age of 11, a dark-adapted single flash ERG performed at another hospital showed that there were reduced responses in both eyes (data not shown). BCVA was 1.2 (with +6.50 dpt., cyl. −2.00 dpt. Ax. 180°) in his right eye and 1.0 (with +7.00 dpt., cyl. −1.50 dpt. Ax. 10°) in his left eye. Fundus examination revealed retinal degeneration of the inferotemporal areas in his right (Figure 2(d)) and left eyes. The OCT images showed that there was marked thinning of the ONL and disruption of the IS/OS line, except

Table 1: The rare variants found in the two Japanese families with *RHO* mutations, focusing on 212 retinal disease-causing genes registered in the RetNet database (https://sph.uth.edu/retnet/).

JU0678-062JIKEI		Gene	Gene Bank ID	Exon	Nucleotide change	AA change	State	SNP ID
Chrom	Position							
2	202498104	*TMEM237*	NM_001044385	5	c.325C>T	p.R109X	Hetero	
3	129249734	*RHO*	NM_000539	2	c.377G>T	p.W126L	Hetero	
4	6290790	*WFS1*	NM_006005	4	c.392T>G	p.V131G	Hetero	
4	6302786	*WFS1*	NM_006005	8	c.1264G>T	p.A422S	Hetero	
7	33427676	*BBS9*	NM_198428	19	c.2035C>T	p.R679W	Hetero	
8	10480476	*RP1L1*	NM_178857	2	c.236G>A	p.R79H	Hetero	
14	21792816	*RPGRIP1*	NM_020366	14	c.1802C>T	p.S601L	Hetero	rs3748360
16	49670817	*ZNF423*	NM_015069	4	c.2243_2245del	p.748_749del	Hetero	
JU0575-037JIKEI		Gene	Gene Bank ID	Exon	Nucleotide change	AA change	State	SNP ID
Chrom	Position							
1	94476477	*ABCA4*	NM_000350	40	c.5593C>T	p.H1865Y	Hetero	rs201707267
2	112751865	*MERTK*	NM_006343	9	c.1334G>A	p.R445Q	Hetero	rs202242962
3	129252550	*RHO*	NM_000539	5	c.1036G>C	p.A346P	Hetero	
11	17531103	*USH1C*	NM_153676	18	c.1813A>C	p.I605L	Hetero	
16	16291933	*ABCC6*	NM_001171	10	c.1283A>G	p.N428S	Hetero	rs201880691

Chrom = choromosome, AA = amino acid, Homo = homozygous, and Hetero = heterozygous.

for the foveal region of his right (Figure 2(d)) and left eyes. GP showed constriction of visual fields with small scotomas in his right (Figure 2(d)) and left eyes. A fundus autofluorescence image revealed a perifoveal hyperautofluorescent ring in his right (Figure 2(e)) and left eyes. He was diagnosed as an early stage of RP.

3.3. Molecular Genetic Findings. The obtained sequence data were analyzed in accordance with the filtering steps discussed in the Material and Methods section. Table 1 summarizes the remaining rare variants that were examined in families 1 and 2. The analysis focused on the 212 retinal disease-causing genes that were listed in the RetNet database. The two *RHO* mutations revealed in the data, c.377G>T, p.W126L in exon 2 and c.1036G>C, p.A346P in exon 5, were found in the adRP patients of families 1 and 2, respectively. With the exception of these *RHO* mutations, there were no other mutations found in the obtained sequence data for both families 1 and 2 that fulfilled the RP phenotype and autosomal dominant inheritance pattern conditions. The p.W126L mutation has not been previously reported in the literature and is not found in the dbSNP (http://www.ncbi.nlm.nih.gov/SNP/), 1000 Genomes database, or the HGMD (http://www.hgmd.org). On the other hand, the p.A346P mutation was previously reported to be the cause of adRP in one Spanish family [34]. We used *in silico* bioinformatics tools to investigate the impact of the p.W126L mutation on the RHO function. Results of the PolyPhen-2 program generated a score of 0.999 (probably damaging), which was close to the maximum value of 1.00, while the SIFT program generated a score of 0 (damaging).

For the cosegregation analysis, we investigated whether six of the family 1 members and four of the family 2 members had either the p.W126L or the p.A346P mutation. Our results revealed there was complete cosegregation of each mutation with the RP phenotype in each family (Figures 1(a) and 1(b)).

3.4. Molecular Modeling and Simulation. By using energy minimization and MD simulations, we investigated the possible effects of the p.W126L mutation on the structure of the human opsin moiety that was represented by either the dark-adapted like (high affinity for 11-*cis*-retinal) or the light-adapted like (high affinity for all-*trans*-retinal) crystal structures. Although the simulation time was limited, all four models examined approached similar levels of equilibria. Because the mutation site W126 is located in the third transmembrane helix (TM3), we analyzed differences in the TM3 backbone and in the nearby helices. In the dark-adapted template, the extracellular and central regions of TM3 did not appear to move significantly during the simulation regardless of the type of side chain (W or L) at position 126 (Figures 4(a) and 4(b)). This result corroborates the previous observation that the p.W126L mutation affected the 11-*cis*-retinal binding only marginally in COS-1 cells [35]. Interestingly, in the light-adapted like template, the TM3 helix within the heptahelical bundle moved differently in the WT and the p.W126L mutant models during the 1 ns simulation (Figures 4(c) and 4(d)). While the WT and the p.W126L mutant models exhibited only marginal changes in the TM3 during the first 300 ps of simulation (data not shown), this helix progressively tilted only in the p.W126L mutant during the subsequent 1 ns of simulation (Figure 4(d)). Persistence of this tilting during longer periods may lead to a decrease in the distance between the cytoplasmic ends of TM3 and TM6 and may affect the signal-transduction properties of the protein. The residue L125, which is next to W126 in bovine rhodopsin, is in contact with a highly conserved phenylalanine in the middle

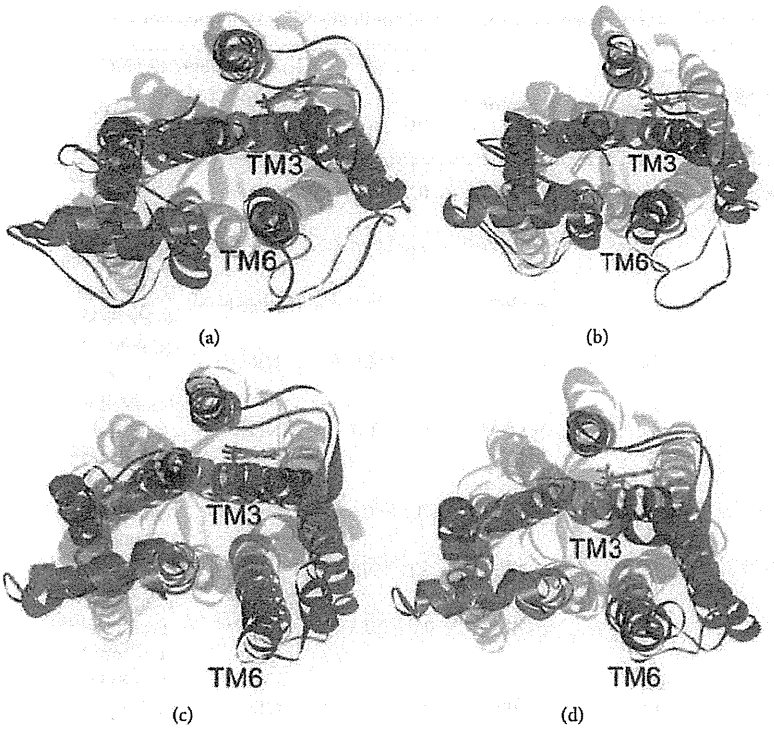

FIGURE 4: Projected view from the cytoplasmic side of the backbone before and after the 1 ns molecular dynamics (MD) simulations. The side chain of the position 126 in each model is shown by the bold sticks in the corresponding colors. (a) Dark-adapted like models. Blue: wild-type after 1 ns MD; green: wild-type before MD. (b) Dark-adapted like models. Red: W126L after 1 ns MD; green: W126L before MD. (c) Light-adapted like models. Blue: wild-type after 1 ns MD; green: wild-type before MD. (d) Light-adapted like models. Red: W126L after 1 ns MD; green: W126L before MD.

of the TM6 at residue 261. These side-chain interactions may therefore be critical for the ligand-induced activation of the rhodopsin-like G-protein-coupled receptors, similar to that which has been proposed for the β2-adrenergic receptor [36].

4. Discussion

In this study, we identified two *RHO* mutations (p.W126L and p.A346P) as disease causes by using whole-exome sequencing in two Japanese families with adRP. We additionally used molecular modeling to analyze the impact of the novel mutation (p.W126L) on the protein structure and function and then evaluated the genotype-phenotype correlations among Japanese RP patients with heterozygous *RHO* mutations.

For the cosegregation analysis, further validation by Sanger sequencing in other family members demonstrated there was complete cosegregation of each mutation with the RP phenotype (Figures 1(a) and 1(b)). For the novel p.W126L mutation, the tryptophan residue at the position 126 is located in the TM3 and is highly conserved among orthologs in vertebrates (Figure 1(c)). A biochemical experiment using reconstituted bovine rhodopsin has shown that an analog of 11-*cis*-retinal is cross-linked to the W126 residue [37]. Our *in silico* study, which used the PolyPhen-2 and SIFT programs, predicted that the p.W126L mutation would cause severe damage to the rhodopsin. In addition, the results of our protein modeling and simulations (Figure 4) suggest that the p.W126L mutation will likely affect the side-chain interaction between TM3 and TM6 in the light-adapted form but will not affect the interaction in the dark-adapted form. These molecular modeling and simulation findings suggest that the p.W126L mutation may impair rhodopsin function by affecting its conformational transition in the light-adapted form. This interpretation is in line with previous studies that have shown that p.W126L of bovine rhodopsin is less potent during G-protein activation [35]. Thus, these results predict that the p.W126L mutation can affect the RHO function, especially in the light-adapted form, thereby leading to the phenotype of RP. On the other hand, p.A346P has previously been reported to be an adRP-causing mutation in one Spanish family [34]. Both our cosegregation data for each family and the molecular modeling confirm that p.W126L is a disease-causing mutation.

With regard to the phenotypes of our patients, the p.W126L (family 1) and p.A346P (family 2) mutations are likely to be associated with sector RP and classic RP, respectively. However, it should be noted that patient III-1 (family 2) was not diagnosed with either classic or sector RP, as patient III-1 exhibited an early stage of RP. The

Table 2: Clinical summary of Japanese patients with autosomal dominant retinitis pigmentosa with heterozygous *RHO* mutations.

Patient, gender	Type of adRP	Age at examination	Mutation	BCVA		Electroretinograms (ERGs)		Reference	Notes
				R	L	Flash (rod plus cone) ERG	Full-field ERG		
Case 1, M	Classic	44	p.P347L	0.5	0.66	NR	NR in 30-Hz flicker	[23, 32]	Cataract
Case 2, F	Classic	20	p.P347L	1.0	1.0	NR	NR in 30-Hz flicker	[23, 32]	
Case 3, F	ND	11	p.P347L	1.0	1.0	Reduced	Reduced in 30-Hz flicker	[23, 32]	
Case 4, F	Classic	75	p.P347L	LP	LP	NR	NR in 30-Hz flicker	[23, 32]	Severe cataract
III-6, M	Sector	49	p.T17M	0.2	0.2	ND	Reduced in both rods and cones	[23, 33]	B-CME, L-CNV
Proband, F	Classic	39	p.E181K	0.1	0.1	ND	NR in rods, reduced in cones	[20]	B-CME
III-5, F	Sector	52	p.N15S	ND	ND	ND	ND	[24]	
II-2, M	Sector	66	p.G106R	0.04	0.5	ND	Reduced in both rods and cones	[25]	R-CME
III-1, F	Sector	44	p.G106R	1.2	1.2	ND	Reduced in rods, normal in cones	[25]	
III-2, F	Sector	40	p.G106R	1.2	1.2	ND	Reduced in rods, normal in cones	[25]	
II-2 (FN.1), M	Sector	58	p.W126L	1.5	0.7	ND	Reduced in both rods and cones	Current study	
III-1 (FN.1), F	Sector	31	p.W126L	1.5	1.2	ND	Reduced in both rods and cones	Current study	
II-1 (FN.2), F	Classic	35	p.A346P	0.7	0.6	ND	NR in both rods and cones	Current study	
III-1 (FN.2), M	ND	14	p.A346P	1.2	1.5	Reduced	ND	Current study	

BCVA = decimal best-corrected visual acuity; R = right eye; L = left eye; B = both eyes; M = male; F = female; FN = family number; ND = not described or not done; NR = nonrecordable; LP = light perception; CNV = choroidal neovascularization; and CME = cystoid macular edema.

phenotypes of patient II-1 (family 2) were similar to those previously reported for a patient of European descent who carried the p.A346P mutation and exhibited classic RP [34]. These findings suggest that the p.A346P mutation might be associated with the phenotype of classic RP.

When trying to diagnose classic or sector RP, it is highly important that one understands the severity and prognosis of *RHO*-associated adRP. As compared to classic RP, sector RP is considered to be a less severe disease with subnormal ERG and visual field defects that correspond to the affected sectors [13, 14]. In fact, it has been reported that sector RP is caused by a number of *RHO* mutations, including p.T4K [38], p.N15S [39–41], p.T17M [33, 42], p.P23H [10], p.T58R [12], p.N78I [43], and G106R [11, 25, 44]. To the best of our knowledge, there have been nine *RHO* mutations reported in the Japanese adRP population [20, 22–25, 32, 33, 41], with detailed phenotypes described in five (p.N15S, p.T17M, p.G106R, p.E181K, and p.P347L) out of the nine mutations [20, 23–25, 32, 33, 41]. Among these five *RHO* mutations, one (p.P347L) exhibited classic RP while the other four (p.N15S, p.T17M, p.G106R, and p.E181K) showed sector RP. Table 2 summarizes the clinical features that were described for the genotype-phenotype correlations of the seven Japanese adRP families (including our families) with the seven *RHO* mutations (p.N15S, p.T17M, p.G106R, p.W126L, p.E181K, p.A346P, and p.P347L). Interestingly, patients with five other mutations (p.N15S [39–41], p.T17M [33, 42], p.G106R [11, 25, 44], p.A346P [34], and p.P347L [5, 32, 45]) were found to have phenotypes that were similar to Japanese and other ethnic groups, although the clinical phenotypes for two

other mutations (p.W126L and p.E181K [20, 21, 46]) could not be sufficiently evaluated [5, 11, 20, 21, 25, 32–34, 39–42, 44–46]. These findings suggest that the location of each missense mutation is important for the purpose of predicting a diagnosis of either classic or sector RP and that there is a similarity of phenotypes between Japanese and other ethnic group RP patients who have identical *RHO* mutations. Also Sandberg et al. report the phenotype-genotype correlations between adRP patients with *RHO* mutations, revealing that patients with mutations altering the intradiscal domain near the N-terminal region (or a low-numbered codon) tended to have better visual function than patients with mutations altering the cytoplasmic domain near the C-terminal region (or a high numbered codon); patients with a mutation altering the transmembrane domain or a mid-numbered codon had intermediate function [47]. Thus, identification of *RHO* mutations appears to be useful for predicting the severity of the RP phenotypes and providing precise genetic counseling.

In conclusion, we identified two *RHO* mutations (p.W126L and p.A346P) in two Japanese families with adRP. The p.W126L mutation has not been previously reported in any ethnic groups. The genotype-phenotype correlations indicated that the location of the *RHO* mutations is likely to determine the phenotype of either classic or sector RP. Identification of *RHO* mutations is a very useful tool for predicting the disease severity and providing precise genetic counseling.

Conflict of Interests

The authors declare there are no conflict of interests.

Acknowledgments

This study was supported by the Grants to Takeshi Iwata from the Ministry of Health, Labor and Welfare of Japan (13803661), to Masakazu Akahori and Takaaki Hayashi from the Ministry of Education, Culture, Sports, Science and Technology of Japan (Grant-in-Aid for Scientific Research C, 25462744 and 25462738), to Takaaki Hayashi from the Vehicle Racing Commemorative Foundation, and to Masaaki Furuno from the research Grant for RIKEN Omics Science Center MEXT. The authors wish to acknowledge RIKEN GeNAS for the sequencing of the exome enriched libraries using the Illumina HiSeq2000.

References

[1] D. T. Hartong, E. L. Berson, and T. P. Dryja, "Retinitis pigmentosa," *The Lancet*, vol. 368, no. 9549, pp. 1795–1809, 2006.

[2] F. C. Mansergh, S. Millington-Ward, A. Kennan et al., "Retinitis pigmentosa and progressive sensorineural hearing loss caused by a C12258A mutation in the mitochondrial MTTS2 gene," *The American Journal of Human Genetics*, vol. 64, no. 4, pp. 971–985, 1999.

[3] K. Kajiwara, E. L. Berson, and T. P. Dryja, "Digenic retinitis pigmentosa due to mutations at the unlinked peripherin/RDS and *ROM1* loci," *Science*, vol. 264, no. 5165, pp. 1604–1608, 1994.

[4] J. Nathans and D. S. Hogness, "Isolation and nucleotide sequence of the gene encoding human rhodopsin," *Proceedings of the National Academy of Sciences of the United States of America*, vol. 81, no. 15 I, pp. 4851–4855, 1984.

[5] T. P. Dryja, T. L. McGee, L. B. Hahn et al., "Mutations within the rhodopsin gene in patients with autosomal dominant retinitis pigmentosa," *The New England Journal of Medicine*, vol. 323, no. 19, pp. 1302–1307, 1990.

[6] T. P. Dryja, T. L. McGee, E. Reichel et al., "A point mutation of the rhodopsin gene in one form of retinitis pigmentosa," *Nature*, vol. 343, no. 6256, pp. 364–366, 1990.

[7] R. E. Stenkamp, D. C. Teller, and K. Palczewski, "Rhodopsin: a structural primer for G-protein coupled receptors," *Archiv der Pharmazie*, vol. 338, no. 5-6, pp. 209–216, 2005.

[8] E. L. Berson, B. Rosner, M. A. Sandberg, and T. P. Dryja, "Ocular findings in patients with autosomal dominant retinitis pigmentosa and a rhodopsin gene defect (Pro-23-His)," *Archives of Ophthalmology*, vol. 109, no. 1, pp. 92–101, 1991.

[9] E. L. Berson, B. Rosner, M. A. Sandberg, C. Weigel-DiFranco, and T. P. Dryja, "Ocular findings in patients with autosomal dominant retinitis pigmentosa and rhodopsin, proline-347-leucine," *The American Journal of Ophthalmology*, vol. 111, no. 5, pp. 614–623, 1991.

[10] J. R. Heckenlively, J. A. Rodriguez, and S. P. Daiger, "Autosomal dominant sectoral retinitis pigmentosa. Two families with transversion mutation in codon 23 of rhodopsin," *Archives of Ophthalmology*, vol. 109, no. 1, pp. 84–91, 1991.

[11] G. A. Fishman, E. M. Stone, L. D. Gilbert, and V. C. Sheffield, "Ocular findings associated with a rhodopsin gene codon 106 mutation: glycine-to-arginine change in autosomal dominant retinitis pigmentosa," *Archives of Ophthalmology*, vol. 110, no. 5, pp. 646–653, 1992.

[12] C. F. Inglehearn, T. J. Keen, R. Bashir et al., "A completed screen for mutations of the rhodopsin gene in a panel of patients with autosomal dominant retinitis pigmentosa," *Human Molecular Genetics*, vol. 1, no. 1, pp. 41–45, 1992.

[13] A. E. Krill, D. Archer, and D. Martin, "Sector retinitis pigmentosa," *American Journal of Ophthalmology*, vol. 69, no. 6, pp. 977–987, 1970.

[14] E. L. Berson and J. Howard, "Temporal aspects of the electroretinogram in sector retinitis pigmentosa," *Archives of Ophthalmology*, vol. 86, no. 6, pp. 653–665, 1971.

[15] R. W. Massof and D. Finkelstein, "Two forms of autosomal dominant primary retinitis pigmentosa," *Documenta Ophthalmologica*, vol. 51, no. 4, pp. 289–346, 1981.

[16] G. B. Bietti, "Su alcune forme atipiche o rare di degenerazione retina (degenerazioni tuppetoretiniche e quardi morbosi similari)," *Boll Oculist*, vol. 16, pp. 1159–1244, 1937.

[17] W. M. Chan, K. Y. Yeung, C. P. Pang et al., "Rhodopsin mutations in Chinese patients with retinitis pigmentosa," *The British Journal of Ophthalmology*, vol. 85, no. 9, pp. 1046–1048, 2001.

[18] Y. Wada and M. Tamai, "Molecular genetic analysis for Japanese patients with autosomal dominant retinitis pigmentosa," *Nippon Ganka Gakkai Zasshi*, vol. 107, no. 11, pp. 687–694, 2003.

[19] K. J. Kim, C. Kim, J. Bok et al., "Spectrum of rhodopsin mutations in Korean patients with retinitis pigmentosa," *Molecular Vision*, vol. 17, pp. 844–853, 2011.

[20] M. Saga, Y. Mashima, K. Akeo, Y. Oguchi, J. Kudoh, and N. Shimizu, "Autosomal dominant retinitis pigmentosa. A mutation in codon 181 (Glu → Lys) of the rhodopsin gene in a

Japanese family," *Ophthalmic Genetics*, vol. 15, no. 2, pp. 61–67, 1994.

[21] T. P. Dryja, L. B. Hahn, G. S. Cowley, T. L. McGee, and E. L. Berson, "Mutation spectrum of the rhodopsin gene among patients with autosomal dominant retinitis pigmentosa," *Proceedings of the National Academy of Sciences of the United States of America*, vol. 88, no. 20, pp. 9370–9374, 1991.

[22] Z.-B. Jin, M. Mandai, T. Yokota et al., "Identifying pathogenic genetic background of simplex or multiplex retinitis pigmentosa patients: a large scale mutation screening study," *Journal of Medical Genetics*, vol. 45, no. 7, pp. 465–472, 2008.

[23] K. Fujiki, Y. Hotta, M. Hayakawa et al., "Point mutations of rhodopsin gene found in Japanese families with autosomal dominant retinitis pigmentosa (ADRP)," *The Japanese Journal of Human Genetics*, vol. 37, no. 2, pp. 125–132, 1992.

[24] K. Fujiki, Y. Hotta, A. Murakami et al., "Missense mutation of rhodopsin gene codon 15 found in Japanese autosomal dominant retinitis pigmentosa," *Japanese Journal of Human Genetics*, vol. 40, no. 3, pp. 271–277, 1995.

[25] M. Matsumoto, S. Hayasaka, T. Yamada, and Y. Hayasaka, "Rhodopsin gene codon 106 mutation (Gly-to-Arg) in a Japanese family with autosomal dominant retinitis pigmentosa," *Japanese Journal of Ophthalmology*, vol. 44, no. 6, pp. 610–614, 2000.

[26] T. Takeuchi, T. Hayashi, M. Bedell, K. Zhang, H. Yamada, and H. Tsuneoka, "A novel haplotype with the R345W mutation in the EFEMP1 gene associated with autosomal dominant drusen in a Japanese family," *Investigative Ophthalmology and Visual Science*, vol. 51, no. 3, pp. 1643–1650, 2010.

[27] S. Katagiri, K. Yoshitake, M. Akahori et al., "Whole-exome sequencing identifies a novel *ALMS1* mutation (p.Q2051X) in two Japanese brothers with Alström syndrome," *Molecular Vision*, vol. 19, pp. 2393–2406, 2013.

[28] P. Emsley, B. Lohkamp, W. G. Scott, and K. Cowtan, "Features and development of Coot," *Acta Crystallographica Section D: Biological Crystallography*, vol. 66, part 4, pp. 486–501, 2010.

[29] W. Humphrey, A. Dalke, and K. Schulten, "VMD: visual molecular dynamics," *Journal of Molecular Graphics*, vol. 14, no. 1, pp. 33–38, 1996.

[30] J. C. Phillips, R. Braun, W. Wang et al., "Scalable molecular dynamics with NAMD," *Journal of Computational Chemistry*, vol. 26, no. 16, pp. 1781–1802, 2005.

[31] T. Darden, D. York, and L. Pedersen, "Particle mesh Ewald: an N·log(N) method for Ewald sums in large systems," *The Journal of Chemical Physics*, vol. 98, no. 12, pp. 10089–10092, 1993.

[32] T. Shiono, Y. Hotta, M. Noro et al., "Clinical features of Japanese family with autosomal dominant retinitis pigmentosa caused by point mutation in codon 347 of rhodopsin gene," *Japanese Journal of Ophthalmology*, vol. 36, no. 1, pp. 69–75, 1992.

[33] M. Hayakawa, Y. Hotta, Y. Imai et al., "Clinical features of autosomal dominant retinitis pigmentosa with rhodopsin gene codon 17 mutation and retinal neovascularization in a Japanese patient," *American Journal of Ophthalmology*, vol. 115, no. 2, pp. 168–173, 1993.

[34] P. M. de Abreu, P. G. Farías, G. S. Paiva, A. M. Almeida, and P. V. Morais, "Persistence of microbial communities including *Pseudomonas aeruginosa* in a hospital environment: a potential health hazard," *BMC Microbiology*, vol. 14, article 118, no. 2, pp. 180–181, 1996.

[35] T. A. Nakayama and H. G. Khorana, "Mapping of the amino acids in membrane-embedded helices that interact with the retinal chromophore in bovine rhodopsin," *The Journal of Biological Chemistry*, vol. 266, no. 7, pp. 4269–4275, 1991.

[36] S. G. F. Rasmussen, H.-J. Choi, J. J. Fung et al., "Structure of a nanobody-stabilized active state of the β_2 adrenoceptor," *Nature*, vol. 469, no. 7329, pp. 175–180, 2011.

[37] T. A. Nakayama and H. G. Khorana, "Orientation of retinal in bovine rhodopsin determined by cross-linking using a photoactivatable analog of 11-cis-retinal," *Journal of Biological Chemistry*, vol. 265, no. 26, pp. 15762–15769, 1990.

[38] L. I. van den Born, M. J. van Schooneveld, L. A. M. S. de Jong et al., "Thr4Lys rhodopsin mutation is associated with autosomal dominant retinitis pigmentosa of the cone-rod type in a small Dutch family," *Ophthalmic Genetics*, vol. 15, no. 2, pp. 51–60, 1994.

[39] H. Kranich, S. Bartkowski, M. J. Denton et al., "Autosomal dominant "sector" retinitis pigmentosa due to a point mutation predicting an Asn-15-Ser substitution of rhodopsin," *Human Molecular Genetics*, vol. 2, no. 6, pp. 813–814, 1993.

[40] L. J. Sullivan, G. S. Makris, P. Dickinson et al., "A new codon 15 rhodopsin gene mutation in autosomal dominant retinitis pigmentosa is associated with sectorial disease," *Archives of Ophthalmology*, vol. 111, no. 11, pp. 1512–1517, 1993.

[41] M. Yoshii, A. Murakami, K. Akeo et al., "Visual function in retinitis pigmentosa related to a codon 15 rhodopsin gene mutation," *Ophthalmic Research*, vol. 30, no. 1, pp. 1–10, 1998.

[42] C. Bell, C. A. Converse, H. M. Hammer, A. Osborne, and N. E. Haites, "Rhodopsin mutations in a Scottish retinitis pigmentosa population, including a novel splice site mutation in intron four," *The British Journal of Ophthalmology*, vol. 78, no. 12, pp. 933–938, 1994.

[43] D. Rivera-De la Parra, J. Cabral-Macias, M. Matias-Florentino, G. Rodriguez-Ruiz, V. Robredo, and J. C. Zenteno, "Rhodopsin p.N78I dominant mutation causing sectorial retinitis pigmentosa in a pedigree with intrafamilial clinical heterogeneity," *Gene*, vol. 519, no. 1, pp. 173–176, 2013.

[44] C. Ayuso, C. Reig, B. Garcia-Sandoval et al., "G106R rhodopsin mutation is also present in Spanish ADRP patients," *Ophthalmic Genetics*, vol. 17, no. 3, pp. 95–101, 1996.

[45] S. Bhattacharya, D. Lester, J. Keen et al., "Retinitis pigmentosa and mutations in rhodopsin," *The Lancet*, vol. 337, no. 8734, p. 185, 1991.

[46] S. Bunge, H. Wedemann, D. David et al., "Molecular analysis and genetic mapping of the rhodopsin gene in families with autosomal dominant retinitis pigmentosa," *Genomics*, vol. 17, no. 1, pp. 230–233, 1993.

[47] M. A. Sandberg, C. Weigel-DiFranco, T. P. Dryja, and E. L. Berson, "Clinical expression correlates with location of rhodopsin mutation in dominant retinitis pigmentosa," *Investigative Ophthalmology & Visual Science*, vol. 36, no. 9, pp. 1934–1942, 1995.

CLINICAL AND EXPERIMENTAL
OPTOMETRY

CLINICAL COMMUNICATION

Fundus autofluorescence findings of acute posterior multifocal placoid pigment epitheliopathy with chronic thyroiditis and splenectomy

Clin Exp Optom 2015; 98: 186–189 DOI:10.1111/cxo.12208

Satoshi Katagiri MD
Yasuhiro Ohkuma MD
Takaaki Hayashi MD PhD
Tamaki Gekka MD PhD
Hiroshi Tsuneoka MD PhD

Department of Ophthalmology, The Jikei University School of Medicine, Tokyo, Japan
E-mail: taka@jikei.ac.jp

Acute posterior multifocal placoid pigment epitheliopathy (APMPPE) was first described by Gass[1] in 1968, as a disease that shows rapid loss of vision due to multifocal, yellow-white, placoid lesions at the level of the pigment epithelium and choroid. The mechanism of APMPPE primarily involves inflammation of the choriocapillaris, with a secondary acute effect on the retinal pigment epithelium that occurs without affecting the intermediate and large choroidal vessels.[2] Several ophthalmic examinations, such as fluorescein angiography, indocyanine green angiography, optical coherence tomography and fundus autofluorescence imaging can be used to diagnose and obtain additional information about APMPPE.[1,3] Fundus autofluorescence imaging has proven to be a useful non-invasive tool, as the fundus autofluorescence signal primarily originates from the lipofuscin accumulation within the retinal pigment epithelium, which reflects its function. Fundus autofluorescence imaging in APMPPE is reported to show characteristic findings that include hypoautofluorescent lesions during the acute phase and increasing hyperautofluorescence during the recovery phase.[3–6]

In this report, we describe a case of unilateral and recurrent APMPPE with a medical history of chronic thyroiditis and splenectomy. Unique fundus autofluorescence findings were observed throughout the clinical course in this patient.

CASE REPORT

A 48-year-old female patient with a history of chronic thyroiditis and splenectomy was referred to our department with a complaint of sudden visual loss in her left eye. The patient reported having mild refractive or anisometropic amblyopia in the left eye and was diagnosed with chronic thyroiditis at the age of 43 years, by ruling out other thyroid-related diseases such as subacute thyroiditis and Graves' disease. After that, the patient was treated with levothyroxine sodium (75 μg daily) and the levels of free T3, free T4 and thyroid stimulating hormone (TSH) have been well controlled within normal ranges. Splenectomy was performed at the age of 44 years due to a splenic artery aneurysm at the hilum of the spleen. No history of recent virus infections was found. At the first examination, decimal visual acuity (VA) was 1.5 with -0.50 DC × 90° in the right eye and 0.7 with +6.00 DS/ -4.25 DC × 55° in the left eye. Using the IOL Master 500 (Carl Zeiss Meditec AG, Dublin, California, USA), her axial lengths were determined to be 22.57 mm in her right and 20.98 mm in her left eye. In both eyes, there were no inflammatory signs found in the anterior segments or media and normal intraocular pressures were observed. Fundus examinations showed no significant findings in her right eye (Figure 1A) and multifocal yellow-white placoid lesions in her left eye (Figure 1B). Fundus autofluorescence imaging (Spectralis HRA; Heidelberg Engineering, Heidelberg, Germany) showed no findings in her right eye (Figure 1C) and a localised hyperautofluorescent lesion along the inferior arcade artery in her left eye (Figure 1D). Although fluorescein angiography showed no abnormal findings in her right eye throughout all of the phases, hypofluorescent spots were observed in her left eye during the early phase (Figure 1E) and hyperfluorescent spots during the late phase (Figure 1F). The fluorescein angiographic pattern of early blockage and late staining of the lesions in her left eye was typical of APMPPE. Indocyanine green angiography showed multiple hypoperfusion spots and a few hyperperfusion spots during both the early (Figure 1G) and late phases (Figure 1H) in her left eye. There were no abnormal findings observed in her right eye.

Fasting venous blood samples were analysed at the first visit. Levels of anti-nuclear antibody (22.5; normal range zero to 19.9), anti-thyroid globulin antibody (over 4,000 U/ml; normal range zero to 27), anti-thyroid peroxidase (over 600 U/ml; normal range zero to 15), and thyroid stimulating hormone receptor antibody (16.0 per cent; normal range zero to 15.0) were all elevated, although the levels of free T3, free T4 and TSH were within normal ranges. Other serological tests, which included anti-DNA antibody, rheumatoid factor, syphilis, toxoplasmosis, measles, herpes, varicella zoster and cytomegalovirus were negative. There was no evidence of systemic inflammation, with the patient found to have a normal erythrocyte sedimentation rate and C-reactive protein levels.

One week after the initial visit to our department, VA was 2.0 and 0.7 in her right and left eyes, respectively. Since the fundus appearance in her left eye worsened, she was started on oral prednisolone (30 mg per day) followed by a three-week taper. Two weeks after the initial visit, placoid lesions of the left fundus (Figure 2A) and the hyperautofluorescent lesions were found to be increasing (Figure 2B). One month after the initial visit, fundus examination showed there were no placoid lesions (Figure 2C) and there was improvement of the hyperautofluorescent lesions (Figure 2D).

Three months after the initial visit, VA was 0.7 in her left eye. Fundus examination and fundus autofluorescence imaging of the

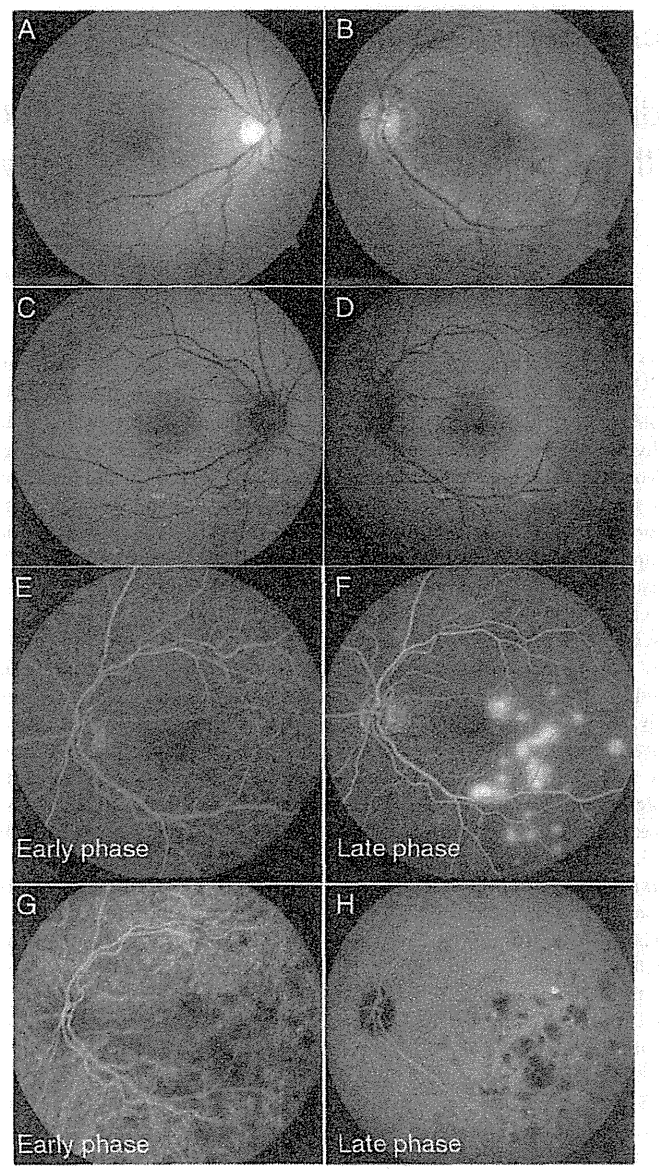

Figure 1. Ophthalmic findings at the patient's initial visit to our department.
Fundus examinations show no remarkable findings in the right eye (A) and multifocal yellow-white placoid lesions in the left eye (B).
Fundus autofluorescence imaging shows no findings in the right eye (C) and a localised hyperautofluorescent lesion along the inferior arcade artery in the left eye (D).
Fluorescence angiographic images of the left eye show hypofluorescent spots during the early phase (E) and hyperfluorescent spots during the late phase (F).
Indocyanine green angiographic images of the left eye show multiple hypoperfusion spots and a few hyperperfusion spots during both the early (G) and the late phases (H).

posterior pole area of her left eye indicated there were no placoid or hyperautofluorescent lesions (Figure 2E,F); however, there were new placoid lesions at the nasal area of her left fundus (Figure 3A). Fundus autofluorescence imaging at the nasal area showed a few hyperautofluorescent lesions (Figure 3B). Therefore, prednisolone (30 mg per day) was restarted, followed by the same three-week tapering used during the initial administration. While fundus examinations showed no placoid lesions in either the posterior pole or nasal area of her left eye at four months after the initial visit (Figure 3C), fundus autofluorescence imaging of the nasal area of her left eye showed several increasing hyperautofluorescent lesions (Figure 3D). Five months after the initial visit, VA was 2.0 and 0.8 in her right and left eyes, respectively. No placoid lesions in the fundus or any hyperautofluorescent lesions were observed in either her right or left eye (Figure 3E,F).

DISCUSSION

Even though fundus photographs, fluorescein angiography and indocyanine green angiography demonstrated there were typical APMPPE findings, the fundus autofluorescence imaging in our current case showed unique findings compared to those in other studies.[3–6] Previous studies have additionally reported that the acute phase showed hypoautofluorescent lesions that corresponded to placoid lesions, with these changes occurring later than those determined by fluorescein angiography and indocyanine green angiography.[3,6] As disease activity subsides, there is increasing autofluorescence around and within the hypoautofluorescent lesions.[3,5] Even at one year after onset, the fundus autofluorescence imaging was reported to show atrophy of the retinal pigment epithelium, which included multiple black spots in the former lesions.[4] In our case, fundus autofluorescence imaging showed there were hyperautofluorescent lesions but no hypoautofluorescent lesions during the acute phase (Figures 2B, 3B). These hyperautofluorescent lesions could be distinguished within a few months (Figures 2F, 3F). Souka and colleagues showed that typical fundus autofluorescence imaging findings depend on the swollen retinal cells that overlay the retinal pigment epithelium.[5] Alternatively, Spaide[6] suggested that this typical fundus autofluorescence is derived

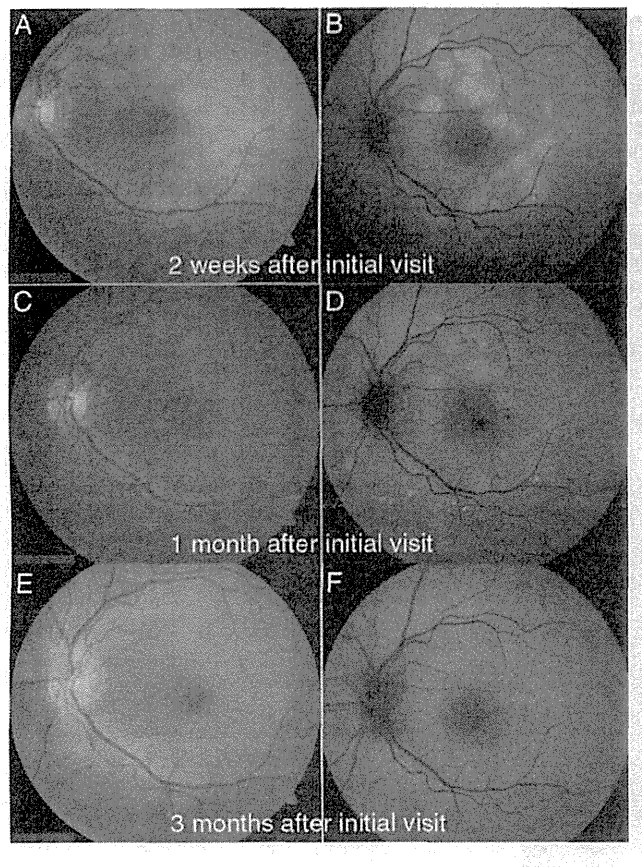

Figure 2. Fundus appearance and fundus autofluorescence imaging at the initial visit.
Two weeks after the initial visit, increases in the placoid lesions of the fundus (A) are observed as compared with the initial visit. Fundus autofluorescence imaging (FAI) also shows increased hyperautofluorescent lesions (B).
One month after the initial visit, fundus examination showed no placoid lesions (C) while the hyperautofluorescent lesions of the FAI were improved (D).
Three months after the initial visit, fundus examination (E) and fundus autofluorescence imaging (F) of the posterior pole area of the left eye showed no placoid or hyperautofluorescent lesions.

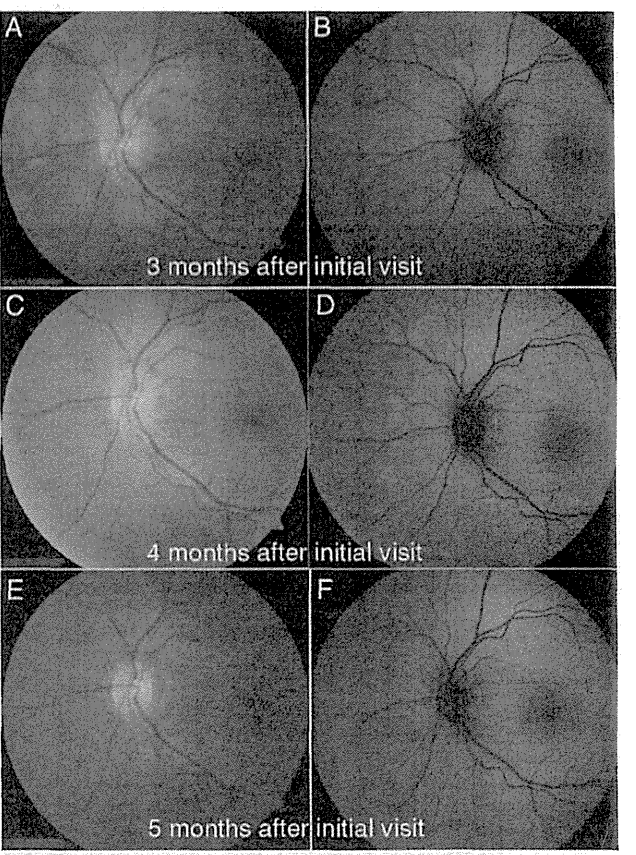

Figure 3. The fundus appearance and fundus autofluorescence imaging at the time of recurrence.
Four months after the initial visit, there are no new placoid lesions in the nasal area of the left eye (A). Fundus autofluorescence imaging of the nasal area shows a few hyperautofluorescent lesions (B).
Four months after the initial visit, while there are no placoid lesions in the nasal area of the left eye (C), the fundus autofluorescence imaging of the nasal area of the left eye show several increasing hyperautofluorescent lesions (D).
Five months after the initial visit, fundus photographs show no placoid lesions (E) and the fundus autofluorescence imaging shows there are no hyperautofluorescent lesions (F).

from the dysfunction of retinal pigment epithelial cells. Hyperautofluorescent lesions observed during the acute phase in our case indicated that the retinal cells were less swollen and/or there was less damage to the retinal pigment epithelial cells compared with previously reported cases.[3–6] In addition, the disappearance of hyperautofluorescent lesions during the recovery phase in our case indicated there was temporary damage to the retinal pigment epithelial cells. Therefore, we considered that these unique fundus autofluorescence imaging findings could be characteristics associated with mild APMPPE cases. Taken together with the fact that the imaging can be measured non-invasively, fundus autofluorescence imaging is a beneficial tool for evaluating the severity of APMPPE.

Currently, APMPPE is considered to have a possible association with thyroid-related diseases, which include subacute thyroiditis and Graves' disease;[7,8] however, to the best of our knowledge, there have been no reports of an association between chronic thyroiditis and APMPPE. Viral infections have been suggested as the cause of APMPPE and subacute thyroiditis, as patients with APMPPE and subacute thyroiditis commonly have

viral infections.[8] On the other hand, the existence of a common autoimmune origin has also been proposed for cases of APMPPE and Graves' disease.[7] Since there is a similar aetiology for chronic thyroiditis and Graves' disease, chronic thyroiditis could be a triggering factor for APMPPE. In addition, in the current case, our patient showed only unilateral APMPPE in her hyperopic left eye. Although it is uncertain why APMPPE occurred unilaterally, the shorter axial length of the left eye compared to the right eye might explain the unilateral presence and subsequent recurrence of APMPPE. It has also been reported that when splenectomies are performed in autoimmune disease patients, this can trigger other autoimmune diseases.[9] Therefore, the splenectomy in our case might have worsened her autoimmune system, thereby partially triggering APMPPE. In summary, the combination of chronic thyroiditis, splenectomy and a short axial length in our patient's left eye is likely to be associated with the observed unilateral and recurrent APMPPE. The decreased vision of the left eye at the final visit may have been due to mild refractive or anisometropic amblyopia.

In conclusion, ophthalmic findings for our current case indicate that fundus autofluorescence imaging is a beneficial tool for evaluating the severity of APMPPE. Furthermore, the combination of chronic thyroiditis, splenectomy and a short axial length may be a trigger of APMPPE.

ACKNOWLEDGEMENTS

This study was supported by grants from the Ministry of Education, Culture, Sports, Science and Technology of Japan (Grant-in-Aid for Scientific Research [C] 25462738 to TH) and the Vehicle Racing Commemorative Foundation (to TH).

REFERENCES

1. Gass JD. Acute posterior multifocal placoid pigment epitheliopathy. *Arch Ophthalmol* 1968; 80: 177–185.
2. Deutman AF, Oosterhuis JA, Boen-Tan TN, Aan de Kerk AL. Acute posterior multifocal placoid pigment epitheliopathy. Pigment epitheliopathy of choriocapillaritis? *Br J Ophthalmol* 1972; 56: 863–874.
3. Steiner S, Goldstein DA. Imaging in the diagnosis and management of APMPPE. *Int Ophthalmol Clin* 2012; 52: 211–219.
4. Framme C, Sachs HG, Gabler B, Roider J. Fundus autofluorescence in APMPPE in association with lyme disease. *Retina* 2002; 22: 653–657.
5. Souka AA, Hillenkamp J, Gora F, Gabel VP, Framme C. Correlation between optical coherence tomography and autofluorescence in acute posterior multifocal placoid pigment epitheliopathy. *Graefes Arch Clin Exp Ophthalmol* 2006; 244: 1219–1223.
6. Spaide RF. Autofluorescence imaging of acute posterior multifocal placoid pigment epitheliopathy. *Retina* 2006; 26: 479–482.
7. Ruiz Vinals AI, Buil Calvo JA, Martinez Giralto O, Castilla Cespedes M. [Acute posterior multifocal placoid pigment epitheliopathy associated with Graves-Basedow's disease]. *Arch Soc Esp Oftalmol* 2002; 77: 381–384.
8. Jacklin HN. Acute posterior multifocal placoid pigment epitheliopathy and thyroiditis. *Arch Ophthalmol* 1977; 95: 995–997.
9. Asherson RA, Gunter K, Daya D, Shoenfeld Y. Multiple autoimmune diseases in a young woman: tuberculosis and splenectomy as possible triggering factors? Another example of the 'mosaic' of autoimmunity. *J Rheumatol* 2008; 35: 1224–1226.

厚生労働科学研究委託費

難治性疾患実用化研究事業

遺伝性網脈絡膜疾患の生体試料の収集・管理・提供と病態解明に関する研究

(H26- 委託(難)- 一般-087)

平成 26 年度　委託業務成果報告書

岩田　岳

平成 27 年 3 月

本報告書は、厚生労働省の科学研究委託事業による委託業務として、独立行政法人 国立病院機構東京医療センターが実施した平成２６年度「遺伝性網脈絡膜疾患の生体試料の収集・管理・提供と病態解明」の成果を取りまとめたものです。